OCU-PHYS 153
March, 1994

Fermilab Library
0 1160 0035397 3

On "Soft photon production rate in resummed perturbation theory of high temperature QCD" — Cancellation of mass singularity

A. NIÉGAWA[1]
Department of Physics, Osaka City University
Sumiyoshi-ku, Osaka 558, Japan

Abstract

Baier, Peigné and Schiff (BPS) have recently reported that the production rate of soft real photons from a hot quark-gluon plasma exhibits unscreened mass singularities even within the hard-thermal-loop (HTL) resummation scheme. It is shown that there exist another diagrams that cancel the singular contribution found by BPS, in accordance with the general theorem of absence of mass singularities in any thermal reaction rate. An interpretation of the relevant diagrams is given in terms of physical processes taking place in a quark-gluon plasma. The mechanism of cancelling mass singularities in this example is quite the same as in vacuum theory. A question is posed on whether the thermal soft photon production rate is physically sensible quantity or not.

[1]E-mail: h1143@ocugw.cc.osaka-cu.ac.jp

FERMILAB
MAR 17 1994
LIBRARY

It has been established by Braaten and Pisarski [1] that, in perturbative thermal QCD, the resummation of the leading-order terms, called hard thermal loops, is necessary. In thermal massless QCD, we encounter the problem of infrared and mass or collinear singularities. The hard-thermal-loop (HTL) resummed propagators soften or screen the infrared singularities, and render otherwise divergent physical quantities finite, if they are not sensitive to a further resummation of the corrections of $\mathcal{O}(g^2T)$. On the other hand, as to the mass singularities, it has been proved [2] that any thermal reaction rates are free from them. (For a compact review of infrared and mass singularities in thermal field theory, we refer to [3].)

The calculation of the production rate of soft real photons ($E = \mathcal{O}(gT)$) from a hot quark-gluon plasma, to $\mathcal{O}(\alpha\alpha_s \ln \alpha_s)$, within the HTL resummation scheme has recently been reported by Baier, Peigné and Schiff (BPS) [4] with the conclusion that the result is divergent, owing to mass singularities. The conclusion seems to contradict the general theorem [2] mentioned above. The purpose of this paper is to show that there are another diagrams which cancel the mass-singular contribution found by BPS, and to give an interpretation of the result in terms of physical processes.

In evaluating the soft-photon production rate, BPS started from the imaginary-time formalism and then continued to the Minkowski space. For the purpose of identifying the physical processes that lead to mass singularities, it is convenient to use the real-time formalism.

After summing over the polarizations of the photon, the production rate is given

by the following two equivalent expressions [5, 6] (see also [7]);

$$W_r = -i\int_\Delta \frac{d^3p}{2E\,(2\pi)^3}\, g_{\mu\nu}\,\Pi_{12}^{\mu\nu}(E,\mathrm{p}) \tag{1}$$

$$= -i\int_\Delta \frac{d^3p}{2E\,(2\pi)^3}\, g_{\mu\nu}^{(t)}(P)\,\Pi_{12}^{\mu\nu}(E,\mathrm{p}), \tag{2}$$

where the subscript r in W_r refers to the "real photon emission", Δ is the small region around the observed photon momentum p, and

$$g_{\mu\nu}^{(t)}(P) = -\sum_{s=1}^{2}\epsilon_\mu^{(s)}(P)\,\epsilon_\nu^{(s)}(P), \tag{3}$$

$$= \tilde{g}_{\mu\nu} + \frac{\tilde{P}_\mu\tilde{P}_\nu}{p^2}, \tag{4}$$

$$\tilde{g}_{\mu\nu} = (0,-1,-1,-1), \quad \tilde{P}_\mu = P_\mu - p_0 N_\mu, \quad N_\mu = (1,\mathbf{0}). \tag{5}$$

In (3), $\epsilon_\mu^{(s)}(P)$ $(s = 1,2)$ is the polarization vector of the photon. [Throughout this paper, a capital letter like P denotes the four momentum, $P = (p_0, \mathrm{p})$, and a lower-case letter like p denotes the length of the three vector, $p = |\mathrm{p}|$. The unit three vector along the direction of, say, p is denoted as $\hat{p} \equiv \mathrm{p}/p$.] In (1) and (2) $\Pi_{12}^{\mu\nu}$ is the $(1,2)$ component of the photon polarization tensor in the real-time formalism based on the time path $C_1 \oplus C_2 \oplus C_3$ in the complex time plane; $C_1 = -\infty \to +\infty$, $C_2 = +\infty \to -\infty$, $C_3 = -\infty \to -\infty - i\beta$ $(\beta = T^{-1})$. [The time-path segment C_3 does not play [8, 9] any explicit role in the present context.] The fields whose time argument are lying on C_1 and on C_2 are referred, respectively, to as the type-1 and type-2 fields. A vertex of type-1 (type-2) fields is called a type-1 (type-2) vertex. Then $\Pi_{12}^{\mu\nu}$ in (1) and (2) is the "thermal vacuum polarization between the type-2 photon and the type-1 photon".

It is worth mentioning that the "Feynman rules" of the above-mentioned real-time formalism is equivalent to the circled diagram rules introduced by Kobes and Semenoff [5], provided that the type-1 (type-2) field is identified with the field of "uncircled" ("circled") type. Thanks to the gauge invariance, (1) and (2) lead to the same result.

The diagrams for W_r that should be considered to leading order are those depicted in Figs.1-3, where $p_0 = E$, and those which are obtained from Figs.2 and 3(a) by reversing the direction of the quark-number flow. In Figs.1-3, i_1, i_2, j_1 and j_2 stand for the type of vertex. In Fig.1, the incoming (outgoing) bare photon-quark vertex is of type-2, $i_1 = 2$ (type-1, $i_2 = 1$), and in Figs.2 and 3, $i_1 = 2$ and $i_2 = 1$ [5, 6]. In Fig.1, all the momenta P, K, K' are soft ($\sim gT$), so that both vertices as well as both quark propagators have to be resummed. In Figs.2 and 3, P and K are soft ($\sim gT$), while Q and R are hard ($\sim T$). It is worth mentioning that Fig.2 includes an effective $\gamma\gamma q\bar{q}$ vertex with HTL, while Fig.3 includes effective $\gamma\gamma gg$ vertices with HTL.

Now the following observations are in order.

• *In the calculation based on the Feynman gauge, eq. (1), Figs.2 and 3 do not yield leading contributions.* This is because the numerator factors, which are obtained after taking the trace of Dirac matrices in the HTL approximation, include the piece $g_{\mu\nu}Q^\mu Q^\nu = Q^2$. The piece which eliminates one of the HTL denominators. Thus the contributions from Figs.2 and 3 are nonleading [1]. This is the reason why Figs.2 and 3 need not to be considered [4] in the calculation by using the Feynman gauge, eq.

(1).

• *In the calculation based on the Coulomb gauge, eq. (2), Figs.1 and 3 do not yield singular contributions.* In the contribution from Fig.1, the mass singularities arise [4] from the factor $1/(E \pm \hat{q}\cdot\mathbf{p})$ that comes from a HTL correction to an effective photon-quark vertex, where $\hat{q} = \mathbf{q}/q$, with $\mathbf{q}$ the hard momentum in the HTL correction. In fact, when $\pm\mathbf{q}||\mathbf{p}$, the above factor potentially yields singularity. Now let us see the numerator factor, which are obtained after taking the trace of Dirac matrices under the HTL approximation. When one of the photon-quark vertices in Fig.1 is the HTL correction and the other is the bare vertex, the numerator is a linear combination of the terms, each of which is of the form $(\hat{q}\cdot\mathbf{a}) - (\hat{q}\cdot\hat{p})(\hat{p}\cdot\mathbf{a})$ with $\mathbf{a}$ being $\mathbf{q}$ or $\mathbf{k}$. Then, the numerator vanishes at $\pm\mathbf{q}||\mathbf{p}$, meaning that there is no singularity. When both photon-quark vertices in Fig.1 are the HTL corrections, there emerges the numerator factor $\hat{q}_1\cdot\hat{q}_2 - (\hat{q}_1\cdot\hat{p})(\hat{p}\cdot\hat{q}_2)$. For $\hat{q}_1 = \pm\hat{p}$ *and* $\hat{q}_2 \neq \pm\hat{p}$, or for $\hat{q}_2 = \pm\hat{p}$ *and* $\hat{q}_1 \neq \pm\hat{p}$, this numerator factor vanishes. For $\hat{q}_1 = \pm\hat{p}$ *and* $\hat{q}_2 = \pm\hat{p}$, the numerator factor gives "double zero". Thus, Fig.1 does not yield singular contribution. That Fig.3 does not yield singular contributions will be briefly discussed at the end of Appendix.

We will use the Coulomb gauge, eq. (2), since this gauge is suitable for the direct physical interpretation. In order to regularize mass singularities, we introduce a small quark mass (cf. the first paragraph of Appendix). Then, we see that the real photon emission diagram that leads to the (mass)-singular contribution in W_r (eq. (2)) is Fig.2 ($p_0 = E$) with $i_1 = j_1 = 2$ *and* $i_2 = j_2 = 1$. Calculational details for evaluating

the singular contribution are given in Appendix. Here we reproduce the result (A.20);

$$\begin{aligned} W_r \;\simeq\; & \frac{2}{\pi} e_q^2 g^2 N_c \frac{N_c^2-1}{2N_c} \int \frac{d^3p}{2E(2\pi)^3} \frac{1}{E^2} \int \frac{d^4K}{(2\pi)^3} n_F(k_0) \\ & \times \sum_{\sigma=\pm} (1-\sigma\hat{q}\cdot\hat{k})\, \rho_\sigma(K) \int \frac{d\Omega}{4\pi} \frac{\delta(k_0 - \hat{p}\cdot\mathbf{k})}{1-\hat{p}\cdot\hat{q}} \\ & \times \int q\, dq \left[n_B(q)\,(1-n_F(q)) + n_F(q)\,(1+n_B(q)) \right], \end{aligned} \tag{6}$$

where the symbol "$\simeq$" is used to denote an approximation that is valid for keeping the singular contributions, and $\rho_\pm$ is the absorptive part of the effective thermal quark propagator, cf. (A.7). In (6), the contribution associated with the first term in the square brackets comes from $Q = (E_q, \mathbf{q})$, while the contribution associated with the second term comes from $Q = (-E_q, -\mathbf{q})$, and the polar angle θ under the integral over the solid angle is defined as $\cos\theta = \hat{p}\cdot\hat{q}$. The Ω integral in (6) diverges at $\cos\theta = 1$ or $\hat{q} = \hat{p}$, which is nothing but the mass singularity.

Carrying out the integrations in (6) over q and over the solid angle Ω with the small quark mass (μ) regulator, we have

$$\begin{aligned} W_r \;\simeq\; & 2\cdot 2\pi e_q^2 N_c m_f^2 \ln\frac{T}{\mu} \int \frac{d^3p}{2E(2\pi)^3} \frac{1}{E} \\ & \times \int \frac{d^4K}{(2\pi)^3} \delta(P\cdot K) \sum_{\sigma=\pm} (1-\sigma\hat{p}\cdot\hat{k})\, \rho_\sigma(K), \end{aligned} \tag{7}$$

where m_f (eq. (A.9)) is the thermal mass of a quark. The factor 2 in front of the right-hand side of (7) reflects the fact that the diagram that is obtained from Fig.2 by reversing the direction of the quark-number flow gives the identical contribution to (6). It is to be noted that, in obtaining (7), we have set $n_F(k_0) = \frac{1}{2}$. This is because, in the HTL approximations, $e^{\beta k_0} = 1 + \mathcal{O}(g)$. Thus, we have reproduced the BPS

result.

For any given diagram in the real-time formalism, general rules of identifying the physical processes are available [6]: Given a (thermal) diagram , like Fig.2, representing some thermal reaction rate may be divided into two parts; the one is the reaction's S-matrix element in *vacuum theory* and the other is the S^*-matrix element. The S- (S^*-) matrix element represents the reaction between the considered particle(s) (the photon in the present case) and the particles in the quark-gluon plasma. The type-1 (type-2) vertices in the thermal diagram go to the vertices in the S- (S^*-) matrix element. The thermal propagator with momentum P from a type-1 vertex to a type-2 vertex is "cut" . When $p_0 > 0$ ($p_0 < 0$) the "cut" is the "final-state cut" ("initial-state cut"). For a thermal propagator from a type-2 vertex to a type-1 vertex, the opposite rule applies. For more details, we refer to [6].

According to the rules outlined above, from Fig.2 (with $i_1 = j_1 = 2$ *and* $i_2 = j_2 = 1$) or (6), we can identify the physical processes. For q_0 ($= E_q$) > 0, for example, the physical process is as depicted in Fig.4; the dot-dashed line is the final-state cut line, the left side part of the cut line represents the S-matrix element in *vacuum theory*, while the right part represents the S^*-matrix element. The group of particles on top of Fig.4 stands for spectators which are constituent particles (quarks, antiquarks and gluons) of the quark-gluon plasma. In Fig.4, two "half blobs" come from the blob on the quark line in Fig.2. Recalling the fact that cutting the blob picks up the Landau damping contribution, we see that there are particles both in the initial

and final states (not drawn explicitly), the particles which connect to each of the two "half blobs". As is seen from (6), when p and q in Fig.4 become collinear, the quark propagator with $P + Q$ diverges, which is the origin of the collinear or mass singularity.

There are another diagrams leading to the singular contributions that cancel (7). The diagrams are Figs.1-3 (and Figs.2 and 3(a) with opposite direction of the quark-number flow) with $i_1 = i_2 = 1$ and with $i_1 = i_2 = 2$. Mass singular contributions appear from these diagrams with $P^2 \sim 0$. Two observations made above in relation to the analysis of real-photon production diagrams also apply to the present case. As a result, the relevant diagrams to be considered are Fig.2 with $j_1 = 2$ *and* $i_1 = i_2 = j_2 = 1$ and with $j_2 = 1$ *and* $i_1 = i_2 = j_1 = 2$. Explicit derivation of the singular contribution is given in Appendix. The result, (A.28), is

$$\begin{aligned} W_v \;\simeq\; & -\frac{2}{\pi} e_q^2 g^2 N_c \frac{N_c^2-1}{2N_c} \int \frac{d^3p}{2E\,(2\pi)^3} \frac{1}{E^2} \int \frac{d^4K}{(2\pi)^3} n_F(k_0) \\ & \times \sum_{\sigma=\pm} (1-\sigma \hat{r}\cdot\hat{k})\, \rho_\sigma(K) \int \frac{d\Omega}{4\pi} \delta(k_0 - \hat{r}\cdot \mathbf{k}) \\ & \times \int r\, dr \left[\frac{n_B(r)\,(1-n_F(r))}{1-\hat{r}\cdot\hat{p}} + \frac{(1+n_B(r))\, n_F(r)}{1+\hat{r}\cdot\hat{p}} \right], \end{aligned} \tag{8}$$

where $r = |\mathbf{r}| = |\mathbf{p}+\mathbf{q}|$ ($\simeq q$), and the subscript v in W_v refers to the "process with virtual photon". For evaluating (8) associated with the second term in the square brackets, we change the integration variable as $\mathbf{p} \to -\mathbf{p}$. Taking into account the contribution from the diagram with opposite direction of the quark-number flow, we obtain $W_v \simeq -W_r$, with W_r as given in (7). Thus, we see that the cancellation of mass singularities occurs between W_r and W_v, $W_r + W_v \simeq 0$. This mechanism of

the cancellation between the mass singularities coming from "real-photon emission" diagram and the "virtual-photon" diagram is essentially the same as in vacuum theory [10].

Now we are in a position to discuss the physical content of the result. Let us identify [6] the physical processes corresponding to Fig.2 with $i_1 = i_2 = j_2 = 1$ *and* $j_1 = 2$. For $q_0 > 0$, the process is as depicted in Fig.5 with the final-state cut line C_2. On the other hand, Fig.2 with $i_1 = i_2 = j_1 = 2$ *and* $j_2 = 1$ corresponds, for $q_0 > 0$, to Fig. 5 with the final-state cut line C_1.

In the real-photon emission process with $q_0 > 0$, Fig.4, the photon in the final state is the particle that we intend to *detect*. However, the quark with momentum **q** in the final state is almost parallel to the momentum of the photon. Then we cannot *detect* the photon only, but inevitably *detect* the photon *and* the quark. Thus we should interpret Fig.4 as giving the production rate of the two-particle state with four momentum $P+Q = R$, which consists of the photon and the quark. On the other hand, in Fig.5, where **r** and **p** is almost parallel (cf. (8)), the quark with momentum $R = P + Q$ is the *detected* particle. This quark has the same momentum and the same quantum number as that of the *detected* quark-photon system in Fig.4. Then, *in the detection process*, we cannot distinguish the processes as depicted in Figs.4 and 5. Thus the physically sensible production rate is given by the sum of both contributions, which is free from mass singularity; $W_r + W_v \simeq 0$.

For the $q_0 < 0$ sector of Fig.2, the situation is the same as above. This type of

"mechanism" of cancelling mass singularities is the familiar one in vacuum theory [10].

Here two comments are in order. (i) The thermal field theory that we employed is formulated for the quark-gluon plasma of infinite extent. So the *detection* mentioned above is to be performed inside the quark-gluon plasma. (ii) One may claim that the actual quark-gluon plasma is of finite extent. The photon (P) in Fig.4 interacts only weakly with quarks and gluons that constitute the plasma, and then it will easily come out of the quark-gluon plasma without further interactions, and one can detect the photon (P) in Fig.4.

We like to make the following two objections against the issue (ii) above. First of all, in order for the photon to come out of the quark-gluon plasma, the "partner" quark (Q) in Fig.4 should interact with other quark(s) and or gluon(s). Such a process is a higher-order process in (improved) perturbative QCD. Then, within the present leading-order approximation, such processes should not be included. Secondly, if we treat seriously the quark-gluon plasma of finite extent, we should make up the perturbative calculational scheme on the basis of single-quark and -gluon eigen-states for the *finite* plasma system [11]. The mass-singularity issue is discussed fully on the basis of the plane-wave eigen-states — the basis for the case of *infinite* plasma. In fact, this "choice" of momentum eigenstates is essential for the appearance of mass singularity. Then, for the case of *finite* plasma, one cannot draw any definite conclusion from the argument based on the plane-wave basis.

From the above argument, it seems rather doubtful whether or not the thermal production rate of a real soft photon is really physically sensible quantity.

Acknowledgement. I sincerely thank R. Baier for useful discussions. Were it not for his criticism on the first draft, this paper would not appear.

Appendix

Derivation of (6)

We consider Fig.2 ($p_0 = E$) with $i_1 = 2$ *and* $i_2 = 1$. Before proceeding to the calculational details, we recall that [12], in order to consistently treat a gauge theory, we should introduce an infrared cutoff, even when the quantity under consideration looks to be free from any singularity. When one is faced with taking two limits, (i) the on-shell limit and (ii) the limit of removing infrared cutoff parameter, one should first take the limit (i). In this paper, as an infrared cutoff, we introduce a small quark mass μ. Keeping this regularization in mind, we will not explicitly write down the quark mass μ except at the final stage (eq. (7) in the text).

Using our regularization, we see that Fig.2 ($p_0 = E$) with $i_1 = 2$ *and* $i_2 = 1$ gives nonzero contribution only when $j_1 = 2$ *and* $j_2 = 1$, which yields

$$
\begin{aligned}
W_r &= -i \int_\Delta \frac{d^3p}{2E\,(2\pi)^3}\, g^{(t)}_{\mu\nu}(P)\, \Pi^{\mu\nu}_{12}(E,\mathbf{p}) \\
&= i e_q^2 g^2 N_c \frac{N_c^2-1}{2N_c} \int \frac{d^4P}{(2\pi)^3}\, \theta(p_0)\, g^{(t)}_{\mu\nu}(P)\, \delta(P^2) \\
&\quad \times \int \frac{d^4K}{(2\pi)^4} \int \frac{d^4Q}{(2\pi)^4}\, \Delta^{\xi\zeta}_{12}(P+Q-K) \\
&\quad \times tr\left[\gamma_\xi\, S_{22}(P+Q)\, \gamma_\mu\, S_{21}(Q)\, \gamma_\nu\, S_{11}(P+Q)\, \gamma_\zeta\, {}^*S_{12}(K)\right], \qquad \text{(A.1)}
\end{aligned}
$$

where Q is of $\mathcal{O}(T)$, while P and K are of $\mathcal{O}(gT)$; $|q^0|$, $q >> |p^0|$, $|k^0|$, $|\mathbf{p}|$, $|\mathbf{k}|$. In (A.1), ${}^*S_{12}$ is the (1-2) component of the effective thermal propagator of a quark. For completeness, we give all the components of ${}^*S_{j\ell}(K)$ $(j,\ell = 1,2)$;

$$
{}^*S_{j\ell}(K) = \sum_{\sigma=\pm} (\gamma\cdot K_\sigma)\, {}^*\tilde{S}^{(\sigma)}_{j\ell}(K), \qquad (j,\ell = 1,2), \qquad \text{(A.2)}
$$

where

$$
K_\sigma = (1, \sigma\hat{k}), \qquad \text{(A.3)}
$$

$$
\begin{aligned}
{}^*\tilde{S}^{(\sigma)}_{11}(K) &= -\left({}^*\tilde{S}^{(\sigma)}_{22}(K)\right)^* \\
&= -\frac{1}{2D_\sigma(K)} + i\pi\,\epsilon(k_0)\, n_F(|k_0|), \qquad \text{(A.4)}
\end{aligned}
$$

$$
{}^*\tilde{S}^{(\sigma)}_{12(21)}(K) = \pm i\pi\, n_F(\pm k_0)\, \rho_\sigma(K), \qquad \text{(A.5)}
$$

with

$$
D_\sigma(K) = -k_0 + \sigma k + \frac{m_f^2}{2k}\left[\left(1-\sigma\frac{k_0}{k}\right)\ln\frac{k_0+k}{k_0-k} + 2\sigma\right], \qquad \text{(A.6)}
$$

$$
\rho_\sigma(K) = \frac{1}{2\pi i}\left[\frac{1}{D_\sigma(k_0+i0,k)} - \frac{1}{D_\sigma(k_0-i0,k)}\right], \qquad \text{(A.7)}
$$

$$
n_F(x) = \frac{1}{e^{\beta x}-1}, \qquad \text{(A.8)}
$$

$$
m_f^2 = \frac{\pi\alpha_s}{2}\frac{N_c^2-1}{2N_c}T^2. \qquad \text{(A.9)}
$$

$D_\sigma(K)$ in (A.6) is first calculated in [13]. Although, the free thermal propagators $S_{j\ell}(K)$ $(j,\ell = 1,2)$ are obtained from (A.2) - (A.9) with $m_f = 0$ and $\rho_\sigma(K) =$

$\delta(k_0 - \sigma k)$, for the purpose of later use, it is convenient to display the "one-term" forms;

$$S_{j\ell}(K) = (\gamma \cdot K)\, \tilde{S}_{j\ell}(K)\,, \tag{A.10}$$

$$\begin{aligned} \tilde{S}_{11}(K) &= -\left\{\tilde{S}_{22}(K)\right\}^*\,, \\ &= \frac{1}{K^2 + i\epsilon} + 2\pi i\, n_F(|k_0|)\, \delta(K^2)\,, \end{aligned} \tag{A.11}$$

$$\tilde{S}_{12(21)}(K) = -2\pi i \left[\theta(\mp k_0) - n_F(|k_0|)\, \delta(K^2)\right]\,. \tag{A.12}$$

The bare thermal gluon propagator $\Delta_{12}^{\xi\zeta}$ in (A.1) is

$$\Delta_{12}^{\xi\zeta}(Q) = -g^{(t)\xi\zeta}(Q)\, \Delta_{12}(Q)\,, \tag{A.13}$$

$$\Delta_{12}(Q) = 2\pi\left[\theta(-q_0) + n_B(|q_0|)\right]\, \delta(Q^2)\,, \tag{A.14}$$

$$n_B(x) = \frac{1}{e^{\beta x} - 1}\,, \tag{A.15}$$

where $g^{(t)\xi\zeta}$ is defined in (4).

Let us write $g_{\mu\nu}^{(t)}(P)$ in (4) as

$$g_{\mu\nu}^{(t)}(P) \equiv g_{\mu\nu} - g_{\mu\nu}^{(\ell)}(P)\,, \tag{A.16}$$

$$g_{\mu\nu}^{(\ell)}(P) = \frac{p^0(N_\mu P_\nu + P_\mu N_\nu) - P_\mu P_\nu}{p^2}\,, \tag{A.17}$$

where N_μ is defined in (5) and use has been made of $P^2 = 0$. Under the HTL approximation, $|q^0|$, $|\mathbf{q}| >> |p^0|$, $|k^0|$, $|\mathbf{p}|$, $|\mathbf{k}|$, it can easily be shown that, in calculating $g_{\mu\nu}\Pi_{12}^{\mu\nu}(P)$, the factor Q^2 appears in the numerator, the factor which eliminates the one hard propagator. Then $g_{\mu\nu}\Pi_{12}^{\mu\nu}(P)$ does not yield a leading contribution [1].

Thus, to leading order, (A.1) is evaluated with the replacement, $g_{\mu\nu}^{(t)} \to -g_{\mu\nu}^{(\ell)}$;

$$W_r = i \int_\Delta \frac{d^3p}{2E\,(2\pi)^3} \left\{\frac{N_\mu P_\nu + P_\mu N_\nu}{E} - \frac{P_\mu P_\nu}{E^2}\right\} \Pi_{12}^{\mu\nu}(E, \mathbf{p})\,. \tag{A.18}$$

The Ward-Takahashi identity simplifies the calculation: We can see first that the $P_\mu P_\nu$ term in (A.18) does not yield singular contributions. Then, the trace calculation under the HTL approximation leads to

$$\begin{aligned} W_r \simeq\ & 8\, i\, e_q^2 g^2 N_c \frac{N_c^2 - 1}{2N_c} \int \frac{d^3p}{2E\,(2\pi)^3} \frac{1}{E} \int \frac{d^4K}{(2\pi)^4} \\ & \times \int \frac{d^4Q}{(2\pi)^4} q^0\, \Delta_{12}^{\xi\zeta}(P + Q - K) \sum_{\sigma=\pm} \left\{Q_\xi K_\zeta^\sigma + Q_\zeta K_\xi^\sigma - g_{\xi\zeta}(Q \cdot K_\sigma)\right\} \\ & \times \left\{\tilde{S}_{11}(P + Q) - \tilde{S}_{22}(P + Q)\right\} \tilde{S}_{21}(Q)\, \tilde{S}_{12}^{(\sigma)}(K)\,, \end{aligned} \tag{A.19}$$

where the symbol "$\simeq$" is used to denote an approximation that is valid for keeping the singular contributions. Replacing $g^{(t)\xi\zeta}(P + Q - K) \simeq g^{(t)\xi\zeta}(Q)$ in $\Delta_{12}^{\xi\zeta}$ with $g^{\xi\zeta} - g^{(\ell)\xi\zeta}(Q)$ as in (A.16) and (A.17), we can easily see that the $g^{(\ell)\xi\zeta}(Q)$ part produces the factor Q^2 in the numerator and yields only nonleading contribution in W_r.

Substituting all the relevant formulae given above into (A.19), after some manipulations, we obtain for the singular contribution,

$$\begin{aligned} W_r \simeq\ & \frac{2}{\pi} e_q^2 g^2 N_c \frac{N_c^2 - 1}{2N_c} \int \frac{d^3p}{2E\,(2\pi)^3} \frac{1}{E^2} \int \frac{d^4K}{(2\pi)^3} n_F(k_0) \\ & \times \sum_{\sigma=\pm} (1 - \sigma \hat{p} \cdot \hat{k})\, \rho_\sigma(K) \int \frac{d\Omega}{4\pi} \frac{\delta(k_0 - \hat{p} \cdot \mathbf{k})}{1 - \hat{p} \cdot \hat{q}} \\ & \times \int q\, dq \left[n_B(q)\,(1 - n_F(q)) + n_F(q)\,(1 + n_B(q))\right]\,, \end{aligned} \tag{A.20}$$

where the contribution associated with the first term in the square brackets comes from $Q = (E_q, \mathbf{q})$, while the contribution associated with the second term comes from

$Q = (-E_q, -\mathbf{q})$. In (A.20), the polar angle θ under the integral over the solid angle is defined as $\cos\theta = \hat{p}\cdot\hat{q}$.

Derivation of (8)

Fig.2 with $i_1 = i_2 = j_2 = 1$ *and* $j_1 = 2$ and with $i_1 = i_2 = j_1 = 2$ *and* $j_2 = 1$ give

$$\begin{aligned} W_v &= e_q^2 g^2 N_c \frac{N_c^2-1}{2N_c} \int \frac{d^4P}{(2\pi)^4} \int \frac{d^4K}{(2\pi)^4} \int \frac{d^4Q}{(2\pi)^4} \Delta_{12}^{\ell\zeta}(P+Q-K) \\ &\quad \times \left[G_{\mu\nu}(P)\, tr\left\{\gamma_\ell\, S_{21}(P+Q)\,\gamma_\mu\, S_{11}(Q)\,\gamma_\nu\, S_{11}(P+Q)\,\gamma_\zeta\, {}^*S_{12}(K)\right\} \right. \\ &\quad \left. - \{G_{\mu\nu}(P)\}^*\, tr\left\{\gamma_\ell\, S_{22}(P+Q)\,\gamma_\mu\, S_{22}(Q)\,\gamma_\nu\, S_{21}(P+Q)\,\gamma_\zeta\, {}^*S_{12}(K)\right\}\right], \end{aligned} \tag{A.21}$$

where

$$G_{\mu\nu}(P) = \frac{g_{\mu\nu}^{(t)}(P)}{P^2+i\epsilon} - \frac{N_\mu N_\nu}{p^2}. \tag{A.22}$$

W_v (eq. (A.21)) develops mass singularity that comes from the region $P^2 \simeq 0$. It can easily be seen that $N_\mu N_\nu/p^2$ parts of the photon propagators do not lead to the singular contributions. We substitute (A.16) with (A.17) for $g_{\mu\nu}^{(t)}(P)$. Just as in the case of eq. (1), we see that the $g_{\mu\nu}$ parts in $g_{\mu\nu}^{(t)}(P)$'s do not yield the leading contributions in W_v (cf. the argument above after (A.17)). Then, we can substitute $-g_{\mu\nu}^{(t)}(P)$ for $g_{\mu\nu}^{(t)}(P)$ in (A.22) that is in (A.21), which again allows us to use the Ward-Takahashi identity. In doing so, we have

$$\begin{aligned} W_v &\simeq -e_q^2 g^2 N_c \frac{N_c^2-1}{2N_c} \int \frac{d^4P}{(2\pi)^4} \frac{p_0}{p^2} \int \frac{d^4K}{(2\pi)^4} \int \frac{d^4R}{(2\pi)^4} \Delta_{12}^{\ell\zeta}(R-K) \\ &\quad \times \left[\frac{1}{P^2+i\epsilon}\, tr\left\{\gamma_\ell\, S_{21}(R)\,\gamma_0\, S_{11}(R-P)\,\gamma_\zeta\, {}^*S_{12}(K)\right\} \right. \\ &\quad \left. + \frac{1}{P^2-i\epsilon}\, tr\left\{\gamma_\ell\, S_{22}(R-P)\,\gamma_0\, S_{21}(R)\,\gamma_\zeta\, {}^*S_{12}(K)\right\}\right], \end{aligned} \tag{A.23}$$

where $R = Q + P$. Only the terms that produce singular contributions are kept in (A.23). By evaluating the trace of the Dirac matrices under the HTL approximation, we obtain

$$\begin{aligned} W_v &\simeq -8 e_q^2 g^2 N_c \frac{N_c^2-1}{2N_c} \int \frac{d^4P}{(2\pi)^4} \frac{p_0}{p^2} \int \frac{d^4K}{(2\pi)^4} \\ &\quad \times \int \frac{d^4R}{(2\pi)^4} \Delta_{12}^{\ell\zeta}(R-K)\, r_0 \sum_{\sigma=\pm} \left[r_\ell K_\zeta^\sigma + r_\zeta K_\ell^\sigma - g_{\ell\zeta}(R\cdot K_\sigma)\right] \\ &\quad \times \tilde{S}_{21}(R)\, {}^*\tilde{S}_{12}^{(\sigma)}(K) \left[\frac{\tilde{S}_{11}(R-P)}{P^2+i\epsilon} - \text{c.c.}\right], \end{aligned} \tag{A.24}$$

where $\tilde{S}_{j\ell}$ is defined in (A.11) and (A. 12) and ${}^*\tilde{S}_{12}^{(\sigma)}$ in (A.5), and c.c. stands for the complex conjugate.

Now we consider the following term in (A.24),

$$\begin{aligned} &\int \frac{dp_0}{2\pi} \frac{p_0}{P^2+i\epsilon} \tilde{S}_{11}(R-P) \\ &\quad = \int \frac{dp_0}{2\pi} \frac{p_0}{P^2+i\epsilon} \left[\frac{1-n_F(|r_0-p_0|)}{(R-P)^2+i\epsilon} + \frac{n_F(|r_0-p_0|)}{(R-P)^2-i\epsilon}\right]. \end{aligned} \tag{A.25}$$

As is well known, the mass singularities manifest themselves as pinch singularities in the complex p_0-plane. The method of extracting such singularities is familiar after the classic work of Cutkosky [14]. We rewrite (A.25) as

$$\begin{aligned} (A.25) &= \int \frac{dp_0}{2\pi} p_0 \left[\frac{1}{P^2 - ip_0\epsilon} - 2\pi i\, \theta(p_0)\, \delta(P^2)\right] \\ &\quad \times \sum_{\sigma=\pm} \left[\{\theta(\sigma) - \sigma\, n_F(|r_0-p_0|)\} \left\{ \frac{1}{(R-P)^2 - i(p_0-r_0)\epsilon} \right.\right. \\ &\quad \left.\left. - 2\pi i\, \epsilon(\sigma)\, \theta(\sigma(p_0-r_0))\, \delta((R-P)^2)\right\}\right]. \end{aligned} \tag{A.26}$$

The products of two advanced propagators in (A.26) do not lead to singular contributions to W_v, because one can avoid singularities in the complex p_0-plane by deforming the integration contour. Since the term $\tilde{S}_{21}(R)$ in (A.24) includes the factor $\delta(R^2)$, with our small quark-mass regularization, P^2 and $(R-P)^2$ in (A.26) cannot vanish simultaneously. Thus we have

$$(A.26) \simeq \frac{i}{4}\left[\epsilon(r_0)\left\{\theta(-r_0)-n_F(|r_0|)\right\}\left\{\frac{1}{r_0|\mathbf{p}|-\mathbf{r}'\cdot\mathbf{p}}-\frac{1}{r_0|\mathbf{p}|+\mathbf{r}\cdot\mathbf{p}}\right\}\right.$$
$$\left.+\frac{1}{r_0|\mathbf{p}|-\mathbf{r}\cdot\mathbf{p}}\right]. \qquad (A.27)$$

In (A.27), three factors $1/(r_0|\mathbf{p}|\pm\mathbf{r}\cdot\mathbf{p})$ produce mass singularities in W_v. The singularities arising from the two factors in the curry brackets in (A.27) cancel each other.

Substituting the last term in (A.27) into (A.24), and using all the relevant formulae given above, we obtain, after some manipulations,

$$W_v \simeq -\frac{2}{\pi}e_q^2 g^2 N_c \frac{N_c^2-1}{2N_c}\int\frac{d^3p}{2E\,(2\pi)^3}\frac{1}{E^2}\int\frac{d^4K}{(2\pi)^3}n_F(k_0)$$
$$\times\sum_{\sigma=\pm}(1-\sigma\hat{r}\cdot\hat{k})\,\rho_\sigma(K)\int\frac{d\Omega}{4\pi}\delta(k_0-\hat{r}\cdot\mathbf{k})$$
$$\times\int r\,dr\left[\frac{n_B(r)\,(1-n_F(r))}{1-\hat{r}\cdot\hat{p}}+\frac{(1+n_B(r))\,n_F(r)}{1+\hat{r}\cdot\hat{p}}\right]. \qquad (A.28)$$

where use has been made of the HTL approximation.

Fig.3

As in the case of Fig.2 (see above after (A.22)), $N_\mu N_\nu/p^2$ ($N_\xi N_\zeta/k^2$) part which is accomanied with the photon (gluon) line with $i_1=i_2=1$ or 2 ($j_1=j_2=1$ or 2)

do not lead to the singular contributions. The same reasoning as above after (A.17) tells us that the $g_{\mu\nu}$ part of $g^{(t)}_{\mu\nu}(P)=g_{\mu\nu}-g^{(\ell)}_{\mu\nu}(P)$ and the $g^{\xi\zeta}$ part of $g^{(t)\xi\zeta}(K)=g^{\xi\zeta}-g^{(\ell)\xi\zeta}(K)$ lead to nonleading contributions. Then, substituting $-g^{(\ell)}_{\mu\nu}(P)$ for $g^{(t)}_{\mu\nu}(P)$ and $-g^{(\ell)\xi\zeta}(K)$ for $g^{(t)\xi\zeta}(K)$, and using the Ward-Takahashi identity twice, we see that Fig.3 do not yield singular contributions in W_r and in W_v.

References

[1] E. Braaten, R. D. Pisarski: Nucl. Phys. B337 (1990) 569; Nucl. Phys. B339 (1990) 310. See also, J. Frenkel, J. C. Taylor: Nucl. Phys. B334 (1990) 199

[2] A. Niégawa: Phys. Rev. Lett. 71 (1993) 3055

[3] M. Le Bellac, P. Reynaud: University of Nice Report No. INLN 93/29, 1993

[4] R. Baier, S. Peigné, D. Schiff: Orsay and Bielefeld University Report No. LPTHE-Orsay 93/46 BI-TP 93/55, November 1993, to be published in Z. Phys. C

[5] R, Kobes, G. W. Semenoff: Nucl. Phys. B272 (1986) 329

[6] A. Niégawa: Phys. Lett. B247 (1990) 351; N. Ashida, H. Nakkagawa, A. Niégawa, H. Yokota: Phys. Rev. D45 (1992) 2066; Ann. Phys. (N.Y.) 215 (1992) 315 [E: 230 (1994) 161]; Asida N.: Int. J. Mod. Phys. A8 (1993) 1729

[7] H. A. Weldon: Phys. Rev. D28 (1983) 2007

[8] N. P. Landsman, Ch. G. van Weert: Phys. Rep. 145 (1987) 141

[9] A. Niégawa: Phys. Rev. D40 (1989) 1199

[10] T. Kinoshita: J. Math. Phys. 3 (1962) 650; in Lectures in Theoretical physics, Vol. IV. New York, London: John Wiley & Sons 1962, p. 121; T. D. Lee, M. Nauenberg: Phys. Rev. 133 (1964) B1549

[11] A. Niégawa, K. Takashiba: Ann. Phys. (N.Y.) 226 (1993) 293 [E: 230 (1994) 162]; to be published in Mod. Phys. Lett. A

[12] A. Rebhan: Phys. Rev. D46 (1992) 4779

[13] V. V. Klimov: Sov. J. Nucl. Phys. 33 (1981) 934; H. A. Weldon: Phys. Rev. D26 (1982) 2789

[14] R. E. Cutkosky: J. Math. Phys. 1 (1960) 429

Figure captions

Fig.1. A diagram contributing to the real-soft-photon production rate. The blobs indicate the effective quark propagators and the effective quark-photon vertices. i_1 and i_2 designate the type of bare photon-quark veretex.

Fig.2. A diagram with HTL, where Q and R are hard ($\sim T$) while P and K are soft ($\sim gT$). i_1, i_2, j_1 and j_2 designate the type of vertex.

Fig.3. Diagrams with HTL, where Q is hard ($\sim T$) while P and K are soft ($\sim gT$).

Fig.4. The physical process taking place in the quark-gluon plasma, which is responsible for the singular contribution to W_r. The left side of the final-state cut line (dot-dashed line) represents the S-matrix element, while the right side represents the S^*-matrix element.

Fig.5. The physical process taking place in the quark-gluon plasma, which is responsible for the singular contribution to W_v. The diagram with the final-state cut line C_1 (C_2) corresponds to Fig.2(a) with $i_1 = i_2 = j_1 = 2$ *and* $j_2 = 1$ ($i_1 = i_2 = j_2 = 1$ *and* $j_1 = 2$).

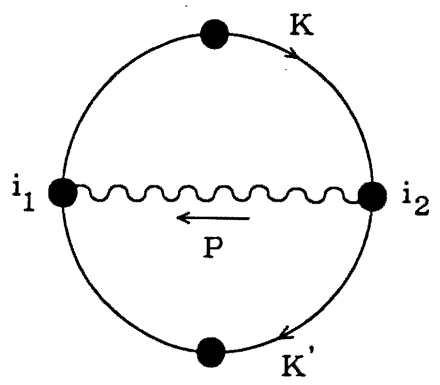

FIG. 1

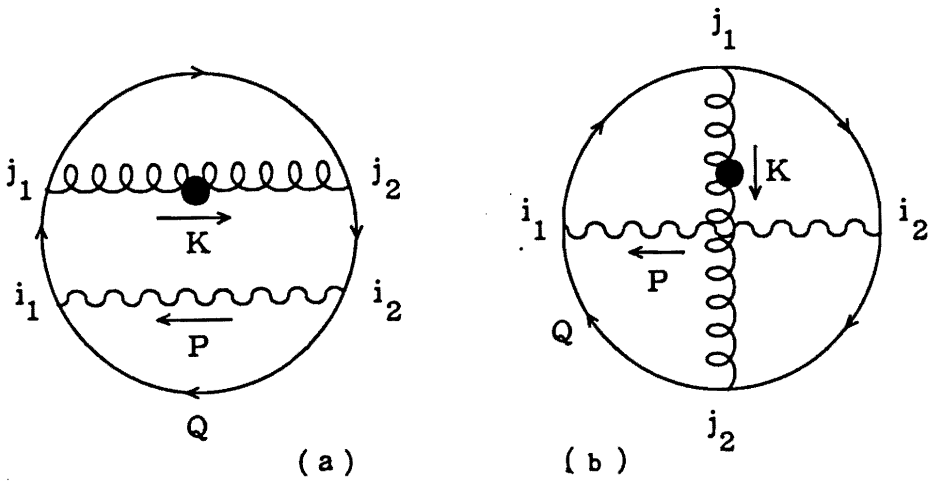

FIG. 3

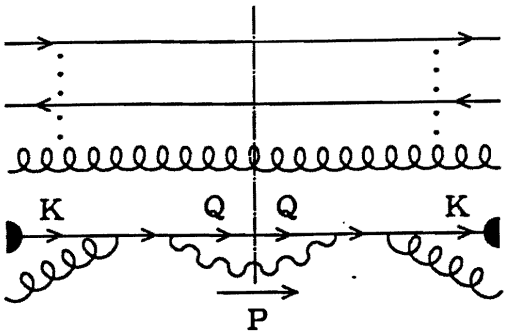

FIG. 4

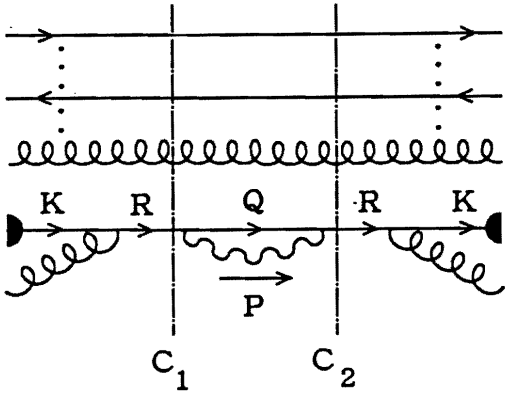

FIG. 5

M.S.
I D No.
NAME
RETURN TO FERMILAB LIBRARY